# Theoretical phase stability of incommensurable spin structures on the {001} surfaces of MnO-type antiferromagnetic semiconductors

D. C. Chrzan and L. M. Falicov
*Department of Physics, University of California, Berkeley, California 94720*
*and Materials and Chemical Sciences Division, Lawrence Berkeley Laboratory, Berkeley, California 94720*
(Received 12 September 1988)

A theory for the phase stability of incommensurable spin structures on the {001} surfaces of the rock-salt–structure antiferromagnetic semiconductors is presented. The theory is based on classical spins and a simple Heisenberg Hamiltonian dependent on three exchange interactions: (a) a surface-only nearest-neighbor exchange; (b) a surface second-layer nearest-neighbor exchange; and (c) an antiferromagnetic second-nearest-neighbor superexchange throughout the crystal. Incommensurable magnetic surface structures are proven to be the ground state for a considerable range of the surface exchange parameters. The properties of the "frozen" spin waves used in the variational calculation are fully explored, and the implications for low-energy electron diffraction studies of the rock-salt–structure antiferromagnets are discussed.

## I. INTRODUCTION

The europium monochalcogenides belong to a class of materials referred to as magnetic semiconductors.[1] These compounds display a variety of magnetic behaviors. In their pure states EuO and EuS are both ferromagnets, EuTe is an antiferromagnet, and EuSe is ferromagnetic below 2.8 K, and antiferromagnetic[2] between 2.8 and 4.6 K.

It is believed that the magnetism in these compounds arises from exchange interactions involving the localized $4f$-shell electrons of the Eu atoms.[1] In the rock-salt structure of Eu$X$ (where $X$ is O, S, Se, or Te), the Eu atoms are located on a face-centered-cubic (fcc) lattice. The varied magnetic structures observed in the Eu$X$ compounds are a consequence of the competition between dipole-dipole interactions[3] and three exchange processes: (i) the direct overlap of the hybridized Eu $4f$-$5d$ orbitals with the 12 neighboring Eu orbitals (generally ferromagnetic); (ii) the superexchange[4] interaction through the valence band formed largely from the $p$ orbitals of the $X$ atoms (antiferromagnetic); and (iii) a nearest-neighbor indirect exchange[5] through the conduction band (either antiferromagnetic or ferromagnetic depending on the amount of doping). Because of the axial nature of the $p$ orbitals of the $X$ atoms, the superexchange mechanism is strongly directed and vanishes for nearest-neighbor Eu atoms.[6] The resulting stable magnetic structures[7] consist of (111) ferromagnetically aligned planes, with alternate planes aligned either parallel (ferromagnets), or antiparallel (antiferromagnets) to each other. The antiferromagnetic structure has been observed[6] in the transition-metal oxides NiO, CoO, MnO, and FeO, and in EuTe.

The surfaces of many of these and related compounds are expected to display anomalous magnetic properties.[8] For example, Castiel[9] calculated the surface magnons of the unreconstructed {001} and {111} surfaces of the Eu$X$ ferromagnets. His calculation predicted soft magnons on both surfaces, demonstrating their tendency to reconstruct magnetically. The calculation involved only normal modes, however, and no attempt was made to calculate the actual ground-state spin structure.

Experimentally, techniques which probe the surface magnetic structure either directly, such as low-energy electron diffraction (LEED),[8,10–12] and spin-polarized low-energy electron diffraction (SPLEED),[8] or indirectly, for example, spin-polarized photoemission,[13–15] have provided valuable experimental results. Photoemission experiments on EuO suggest the presence of a paramagnetic sheet on its {001} surfaces.[16,17] SPLEED studies of Gd give a surface Curie transition temperature a full 22 K above the bulk value.[18] In the experiment which prompted this research,[19] Grazhulis and collaborators report the appearance of symmetry-breaking incommensurable surface spin-structures with temperature-dependent wave vectors in low-temperature ($\approx 10$ K) low-energy electron diffraction studies of single-crystal EuTe{001} surfaces obtained by cleavage under ultrahigh-vacuum conditions.

The stability of incommensurable spin-density waves in some metals, such as Cr, is usually attributed to Fermi-surface–type effects,[20–23] but EuTe, a semiconductor, has no Fermi surface.

The calculation presented here (preliminary results of this calculation appeared in a previous publication[24]) demonstrates that the stability of the incommensurable magnetic structures on the {001} surfaces of EuTe, observed by Grazhulis and co-workers, most likely originates in the competition between relatively large surface nearest-neighbor exchanges and the second-nearest-neighbor superexchange interactions characteristic of the bulk. [This possibility has been clearly demonstrated in similar systems; e.g., the axial next-nearest-neighbor Ising (ANNNI) model[25,26] predicts the stability of long-period structures in its phase diagram.] The calculation, based on a classical Heisenberg Hamiltonian at zero temperature, including all possible commensurable structures

 

plus one class of incommensurable surface spin arrangements, yields a complex phase-stability diagram (as a function of surface exchange integrals) with regions of commensurable and incommensurable ground-state structures. There is no need to introduce either mean-field interactions or potentials incommensurable with the lattice to stabilize the incommensurable structures.[23,27,28]

Section II deals with the details of the model and the calculation, Sec. III contains the results and discussion, and Sec. IV presents the conclusions.

## II. CALCULATIONS

The Eu atoms of the (001) surface of EuTe are sketched in Fig. 1. The orientation shown for the spins are those chosen for the bulk antiferromagnet.[29] Three exchange integrals enter the calculation: $J$, the superexchange between second-nearest neighbors throughout the crystal; $K$, the net exchange between nearest neighbors on the surface; and $L$, the net exchange between nearest neighbors where one atom is in the surface layer, and the other is in the second layer. Because only the antiferromagnets are considered, $J$ is restricted to be positive, but $K$ and $L$ are allowed to have either sign. Nearest-neighbor exchange in the bulk is neglected and all layers, except the two surface layers, are assumed to have the bulk antiferromagnetic configuration. The total energy is written

$$E = J \sum_{(ij)} \mathbf{S}_i \cdot \mathbf{S}_j + K \sum_{\langle ij \rangle} \mathbf{S}_i \cdot \mathbf{S}_j + L \sum_{[ij]} \mathbf{S}_i \cdot \mathbf{S}_j \ , \tag{1}$$

where $\mathbf{S}_i$ is a classical spin of unit magnitude fixed at site $i$, $(ij)$ designates a second-nearest-neighbor pair, $\langle ij \rangle$ is a nearest-neighbor pair with both spins at the surface, and $[ij]$ is a nearest-neighbor pair with one spin at the surface and one in the second layer; the sums run over an infinite half-space.

Exchange interactions depend quite sensitively on a variety of parameters including pressure, doping, temperature, and proximity to a surface.[1,8,30,31] While the low temperatures in the experiments of Grazhulis and coworkers imply that the entropy term of the free energy can be neglected relative to the internal energy, the properties of EuSe suggest that the exchange interactions in the europium monochalcogenides are still very sensitive to changes in temperature. This temperature dependence is, then, accurately modeled by a change in the exchange interactions at zero temperature. Additionally, the nearest-neighbor surface exchange is more sensitive to the effects of the loss of three-dimensional symmetry at the surface, as reflected in the electronic structure and the buckling of the surface, than the second-nearest-neighbor superexchange. This model, therefore, investi-

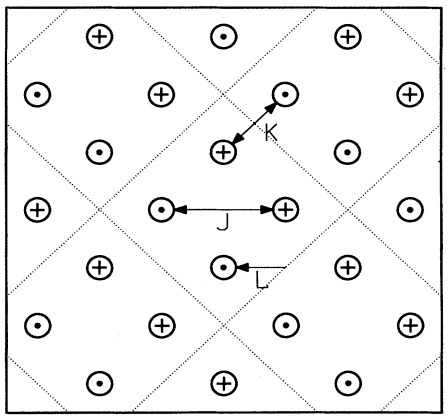


FIG. 1. The Eu atoms of the (001) surface layer of EuTe. The spins of the europium atoms are indicated in stereographic projections, with dots pointing upwards and crosses pointing downwards. The spins are depicted in the chosen bulk configuration (one domain). The arrow labeled $J$ represents the second-nearest-neighbor superexchange interaction and the arrow labeled $K$ represents the nearest-neighbor interaction, effective among surface atoms only. The nearest-neighbor interaction between a surface europium atom and its four nearest neighbors in the layer below (not shown) is represented by the arrow $L$.

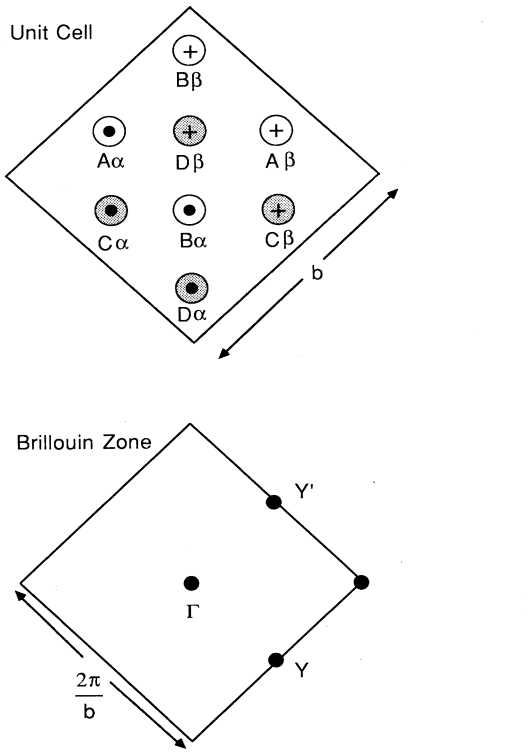


FIG. 2. The unit cell and the Brillouin zone used for the calculation. All spins (indicated in stereographic projections as in Fig. 1) are in the chosen bulk configuration. The square unit cell has linear dimension $b$. The first label on each atom refers to each of the four simple-cubic sublattices, and the Greek label refers to each of the two face-centered-cubic sub-sublattices. The shaded atoms (labeled $C$ and $D$) lie in the layer immediately below the surface; the remaining pictured spins (labeled $A$ and $B$) are in the surface layer. The $\Gamma$ point corresponds to all the so-called commensurable structures. The points $Y$ and $Y'$ are not equivalent because of the asymmetry of the bulk spin domain structure.

gates a range of surface exchange interactions, measured relative to the bulk superexchange strength.

The two-dimensional unit cell chosen for the calculation contains four atoms from each plane. The cell, with linear dimension $b$, and its Brillouin zone are shown in Fig. 2. (The spins are depicted in the chosen bulk configuration.) The points $Y$ and $Y'$ in the Brillouin zone are not equivalent because the spin domain structure of the bulk introduces a preferred direction on the surface.

The Eu face-centered-cubic lattice is divided into four interpenetrating simple-cubic lattices, each of which is further divided into two interpenetrating face-centered-cubic lattices. Each simple-cubic sublattice is denoted by a subscript $i$ which runs from $A$ to $D$. Each face-centered-cubic sub-sublattice corresponding to a given simple-cubic sublattice is designated by the subscript $\mu$, which is either $\alpha$ or $\beta$.

The trial spin configurations in the two topmost layers have the form of a "frozen," finite-amplitude spin wave:

$$\mathbf{S}_{i\mu}(\mathbf{R})=x_{i\mu}\cos(\mathbf{k}\cdot\mathbf{R}+\phi_{i\mu})\hat{\mathbf{x}} +y_{i\mu}\sin(\mathbf{k}\cdot\mathbf{R}+\phi_{i\mu})\hat{\mathbf{y}}+z_{i\mu}\hat{\mathbf{z}}\ , \qquad x_{i\mu}^2=y_{i\mu}^2=1-z_{i\mu}^2 \tag{2}$$

where $\hat{\mathbf{z}}$ is a unit vector in the direction of the bulk spins, $\mathbf{R}$ refers to the position of the unit cell, and $\mathbf{k}$ lies in the Brillouin zone of Fig. 2. States with $\mathbf{k}=\mathbf{0}$ are referred to as commensurable, and states with $\mathbf{k}\neq\mathbf{0}$ are called incommensurable. The spins of (2) have magnitude unity and the energy given by (1) and (2) is easily summed to obtain a closed expression for the energy per unit cell for all $\mathbf{k}$, including those at the zone edge.

All spins not in the top two layers are kept fixed:

$$x_{i\mu}=y_{i\mu}=0\ , \tag{3a}$$

and

$$z_{i\alpha}=1,\quad z_{i\beta}=-1\ . \tag{3b}$$

The total energy (1) and (2), for given values of $K/J$ and $L/J$ in the range $-5\le K/J\le 5$ and $-5\le L/J\le 5$, is minimized with respect to $x_{i\mu}$, $y_{i\mu}$, $\phi_{i\mu}$ and $\mathbf{k}$.

## III. RESULTS AND DISCUSSION

The minimum-energy phase stability diagram for commensurable structures ($\mathbf{k}=\mathbf{0}$) is shown in Fig. 3. The contours are those of constant energy per unit cell of the two surface layers, measured in units of $J$. The dark lines represent phase boundaries of second or higher order: the orientations of the spins change continuously with $K/J$ and $L/J$.

The simply truncated bulk phase (Fig. 1) is the lowest-energy commensurable spin structure in region I of parameter space. The two surface layers of this phase have energy per unit cell $-24J$.

The minimum-energy commensurable spin structure in region II can be described analytically in terms of the parameter $K/J$. The second-layer spins with $i=C,D$ are in the bulk configuration (3); the first-layer spins are given by

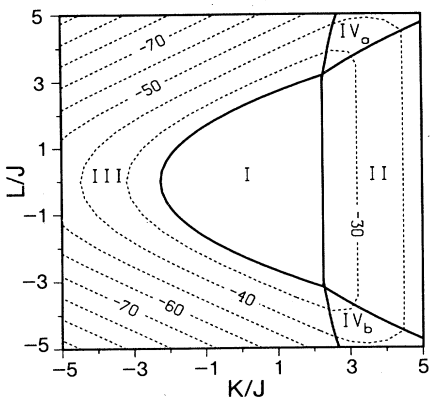


FIG. 3. The phase-stability diagram for commensurable structures. Region I is the unreconstructed, bulklike surface. In region II the various spins acquire an $xy$ component. In the limit $K/J\to\infty$ the surface is a perfect nearest-neighbor square antiferromagnet (NNSA), with surface spins aligned in the $xy$ plane and each surface spin aligned antiparallel to its four nearest-neighbors in the surface layer. Region III is similar, but with the surface spins tilting toward a ferromagnetic surface configuration. Regions $IV_a$ and $IV_b$ correspond to a more complicated spiral-type arrangement of the spins. The contours are those for constant energies (per unit cell, in units of $J$) of the two surface layers of the lowest-energy commensurable states.

$$\begin{aligned}
\mathbf{S}_{A\alpha}(\mathbf{R})&=[1-(4K/J-8)^{-2}]^{1/2}\hat{\mathbf{x}}+(4K/J-8)^{-1}\hat{\mathbf{z}}\ ,\\
\mathbf{S}_{B\alpha}(\mathbf{R})&=-[1-(4K/J-8)^{-2}]^{1/2}\hat{\mathbf{x}}+(4K/J-8)^{-1}\hat{\mathbf{z}}\ ,\\
\mathbf{S}_{A\beta}(\mathbf{R})&=[1-(4K/J-8)^{-2}]^{1/2}\hat{\mathbf{x}}-(4K/J-8)^{-1}\hat{\mathbf{z}}\ ,\\
S_{B\beta}(\mathbf{R})&=-[1-(4K/J-8)^{-2}]^{1/2}\hat{\mathbf{x}}-(4K/J-8)^{-1}\hat{\mathbf{z}}\ .
\end{aligned} \tag{4}$$

The expression for the energy per unit cell of the two surface layers is

$$E=-8K/J-4-(2K/J-4)^{-1}\ . \tag{5}$$

The I-II boundary is at $K/J=2.25$. As $K/J$ is increased, with $L/J$ held constant, the spins tend progressively toward the nearest-neighbor square antiferromagnet (NNSA) in which every surface spin is aligned exactly antiparallel to its four nearest-neighbor surface spins, and all surface spins lie in the (001) plane. The configuration of the surface spins for $K/J=2.50$ is shown in Fig. 4, and Table I displays the corresponding values of the variational parameters of Eq. (2). (The units and coordinate system used for $\mathbf{k}$ in this and all further tables are such that the points $Y'$ and $Y$ are given by [0.000, 0.500] and [0.500, 0.000], respectively.)

The variational parameters for a spin configuration typical of region III are given in Table II. In this region, the spins in each of the two surface planes have their $z$ components aligned in the bulk configuration, and their $xy$ components aligned ferromagnetically. The two surface planes then align with $xy$ components antiparallel ($L/J>0$) or parallel ($L/J<0$). The canting of the spins in both the surface layer and the second layer depends on $L/J$ and $K/J$. A positive value for $K/J$ should result in

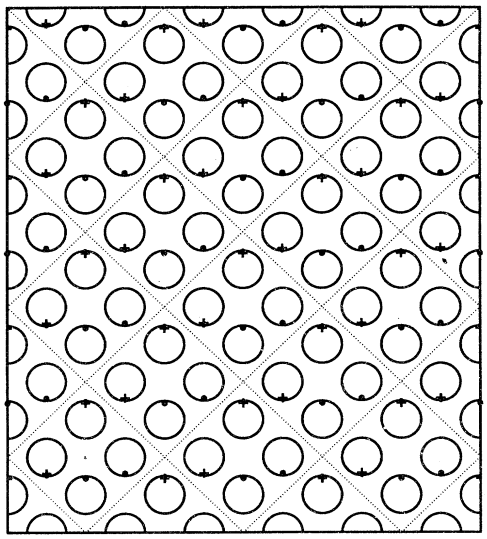

FIG. 4. A stereographic projection of the surface spins for a structure typical of region II, corresponding to the spin parameters in Table I. The dots denote spins pointing up, and the crosses spins pointing down. The tendency toward NNSA in this state is clearly evident.

partial NNSA alignment of the surface spins, except when the $L/J$ interaction overwhelms the $K/J$ interaction, as it does in region III. For $K/J<0$, there is no competition between the two types of nearest-neighbor interactions; both interactions favor partially ferromagnetic alignment of the surface spins.

The regions labeled $IV_a$ and $IV_b$ display the most complicated behavior of all the commensurable structures. Table III contains the parameters describing the stable structure at the point $K/J=3.0$, $L/J=4.0$. The surface layer is in a spiral-type state and the second-layer spins are aligned in a fashion similar to the second-layer spins in region III, i.e., mostly antiparallel to the surface layer for $L/J>0$ in region $IV_a$, and mostly parallel to the surface layer for $L/J<0$ in region $IV_b$. This configuration is the result of the "frustration" arising from the competition between $K/J$ and $L/J$.

The $\pm(L/J)$ symmetry of Fig. 3 is easily understood. As stated above, the nearest-neighbor interplane exchange tends to align the in-plane components of the spins in each of the two (001) planes nearest to the surface ferromagnetically. The symmetry in $\pm(L/J)$ stems from the fact that the two partially ferromagnetic surface planes can align in either of two directions: ferromagnetically or antiferromagnetically, depending on the sign of $L/J$. Even though the configurations of the spins are drastically different for $\pm(L/J)$, the resulting minimum energies are identical. (This symmetry continues to hold when incommensurable structures are included in the calculation, although the configurations are considerably more complicated.)

Inclusion of incommensurable spin structures [$\mathbf{k}\neq\mathbf{0}$ in (2)] yields the phase-stability diagram of Fig. 5. The most notable difference from Fig. 3 is the appearance of the two shaded regions in which the structures of minimum energy are incommensurable with the underlying lattice. Because all commensurable structures have been included and explicitly calculated, the ground state in the shaded regions is guaranteed to be incommensurable. Since the trial state (2) does *not* include *all possible incommensurable structures,* the true *incommensurable* ground states may be different from the ones reported here.

The structures labeled i, ii, and iii are equivalent to those labeled I, II, and III in Fig. 3. The incommensurable structures are of two types, labeled iv and v. The stable structures in regions iv are the finite-amplitude "frozen" spin waves, whose $z$ components are reminiscent of the bulk antiferromagnetic state. The structures appearing in regions v are also the frozen spin waves, but their $z$ components are suggestive of a cross between the bulk-antiferromagnetic state and state similar to NNSA, but with the spins all pointing in the $\pm z$ direction instead

TABLE I. Surface spins typical of region II. $K/J=2.5$, $\mathbf{k}=[0,0]$, and the surface energy per unit cell is $-24.6145J$.

| $i\mu$ | $x_{i\mu}$ | $y_{i\mu}$ | $z_{i\mu}$ | $\phi_{i\mu}$ |
|---|---|---|---|---|
| $A\alpha$ | 0.8660 | 0.8660 | 0.5000 | 0.0000 |
| $A\beta$ | 0.8660 | 0.8660 | −0.5000 | 0.0000 |
| $B\alpha$ | −0.8660 | 0.8660 | 0.5000 | 0.0000 |
| $B\beta$ | −0.8660 | 0.8660 | −0.5000 | 0.0000 |
| $C\alpha$ | 0.0000 | 0.0000 | 1.0000 | 0.0000 |
| $C\beta$ | 0.0000 | 0.0000 | −1.0000 | 0.0000 |
| $D\alpha$ | 0.0000 | 0.0000 | 1.0000 | 0.0000 |
| $D\beta$ | 0.0000 | 0.0000 | −1.0000 | 0.0000 |

TABLE II. Surface spins typical of region III. $K/J=-2.50$, $L/J=2.50$, and $\mathbf{k}=[0,0]$, and the surface energy per unit cell is $-45.0090J$.

| $i\mu$ | $x_{i\mu}$ | $y_{i\mu}$ | $z_{i\mu}$ | $\phi_{i\mu}$ |
|---|---|---|---|---|
| $A\alpha$ | 0.9961 | 0.9961 | 0.0882 | 0.0409 |
| $A\beta$ | 0.9961 | 0.9961 | −0.0882 | 0.0409 |
| $B\alpha$ | 0.9961 | 0.9961 | 0.0882 | 0.0409 |
| $B\beta$ | 0.9961 | 0.9961 | −0.0882 | 0.0409 |
| $C\alpha$ | −0.9993 | −0.9993 | 0.0368 | 0.0409 |
| $C\beta$ | −0.9993 | −0.9993 | −0.0368 | 0.0409 |
| $D\alpha$ | −0.9993 | −0.9993 | 0.0368 | 0.0409 |
| $D\beta$ | −0.9993 | −0.9993 | −0.0368 | 0.0409 |

TABLE III. Surface spins typical of region IV. $K/J=3.00$ and $L/J=4.00$, $\mathbf{k}=[0,0]$, and the surface energy per unit cell is $-30.5833J$.

| $i\mu$ | $x_{i\mu}$ | $y_{i\mu}$ | $z_{i\mu}$ | $\phi_{i\mu}$ |
|---|---|---|---|---|
| $A\alpha$ | 0.9683 | 0.9683 | 0.2499 | 0.8872 |
| $A\beta$ | 0.9683 | 0.9683 | −0.2499 | 0.8872 |
| $B\alpha$ | 0.9683 | −0.9683 | 0.2499 | 0.8700 |
| $B\beta$ | 0.9683 | −0.9683 | −0.2499 | 0.8700 |
| $C\alpha$ | 0.9270 | −0.9270 | 0.3751 | 0.0085 |
| $C\beta$ | 0.9270 | −0.9270 | −0.3751 | 0.0085 |
| $D\alpha$ | 0.9270 | −0.9270 | 0.3751 | 0.0085 |
| $D\beta$ | 0.9270 | −0.9270 | −0.3751 | 0.0085 |

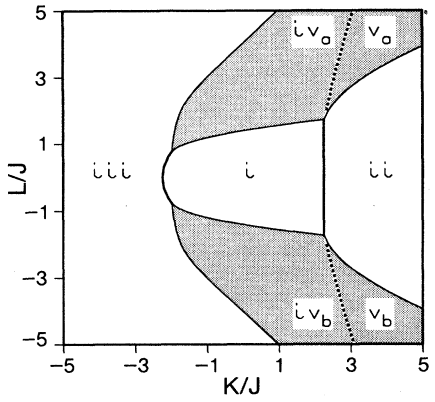


FIG. 5. The phase-stability diagram for all examined structures. Regions i, ii, and iii are commensurable structures identical to the corresponding structures of Fig. 3. The shaded regions are incommensurable structures. The incommensurable structures all, as found, have a single **k** vector. The regions iv have an extra degeneracy not present in regions v.

of lying in the $xy$ plane ($z$-NNSA). As in the commensurable case, the subscripts a and b refer to the manner in which the second-layer spins align themselves with the surface layer, i.e., generally antiparallel or parallel, respectively. Typical spin parameters for these two regions are given in Tables IV, V, and VI. Figures 6, 7, and 8 are the incommensurable spin structures corresponding to the parameters of Tables IV–VI, respectively. The structures in Figs. 6 and 7 have the same energy, even though their **k** vectors are orthogonal to each other.

The **k** vectors of the minimum-energy incommensurable states lie along either the line from $\Gamma$ to $Y$ or the line from $\Gamma$ to $Y'$ (Fig. 2). By symmetry, the minimum-energy states with wave vectors $\pm\mathbf{k}$ are degenerate. The structures in regions iv have an additional degeneracy: the minimum-energy state with wave vector on the line from $\Gamma$ to $Y$ is degenerate with the state with wave vector of the same magnitude on the line from $\Gamma$ to $Y'$. This degeneracy is somewhat surprising, given the domain asymmetry of the bulk configuration, but it can be understood as follows. The Heisenberg interactions only couple respective components of the two spins: the $x$ component of one spin is coupled to the $x$ component of another, and so on. The asymmetry of the bulk lies entirely in the $z$ component of the spins. Since the $z$ components of the spins do not depend directly on **k**, one might expect the $\Gamma$-to-$Y$ and $\Gamma$-to-$Y'$ directions to be equivalent. This is certainly true if the $z$ components of all the spins in a given layer have the same magnitude, as they do in regions iv. If, however, the $z$ components of a given plane are not of uniform magnitude, as in regions v, the asymmetry of the bulk is felt through the corresponding magnitudes of the $xy$ components of the spins, which are also no longer uniform. These $xy$ components do depend directly on **k**, and so the $\Gamma$-to-$Y$ and $\Gamma$-to-$Y'$ directions are not equivalent. Examination of Tables IV–VI and Figs. 6–8 reveal that the conditions for the additional degeneracy are fulfilled in regions iv but not in regions v. The interaction responsible for lifting the degeneracy in regions v is $K$, the nearest-neighbor surface interaction. The observed $z$-NNSA-bulk mixed state is a configuration resulting from the compromise between a large antiferromagnetic $K$ and the constraints imposed by Eq. (2).

The i-iv and ii-v boundaries of Fig. 5 are first-order transitions: **k** goes discontinuously from zero to a finite value at the boundary. The $xy$ amplitudes of the frozen spin waves increase continuously from zero to a finite value. The iii-iv boundaries represent higher-order transitions. The iv-v boundaries are more complicated: the $xy$ amplitudes change continuously across the boundary, as does the magnitude of **k**, but the degeneracy goes from fourfold to twofold when crossing from regions iv into regions v.

The value of **k** for the minimum-energy state can be very sensitive to changes in the surface exchange integrals. Extreme sensitivity occurs in the region of pa-

TABLE V. Surface spins typical of region iv$_a$. $K/J=2.25$ and $L/J=2.25$, $\mathbf{k}=[0.2445, 0.0000]$, and the surface energy per unit cell is $-25.0471J$.

| $i\mu$ | $x_{i\mu}$ | $y_{i\mu}$ | $z_{i\mu}$ | $\phi_{i\mu}$ |
|---|---|---|---|---|
| $A\alpha$ | −0.7321 | −0.7321 | 0.6812 | 0.0000 |
| $A\beta$ | −0.7321 | −0.7321 | −0.6812 | −2.3734 |
| $B\alpha$ | −0.7321 | −0.7321 | 0.6812 | −2.3734 |
| $B\beta$ | −0.7321 | −0.7321 | −0.6812 | 0.0000 |
| $C\alpha$ | 0.8369 | 0.8369 | 0.5474 | −1.1867 |
| $C\beta$ | 0.8369 | 0.8369 | −0.5474 | −3.5600 |
| $D\alpha$ | 0.8369 | 0.8369 | 0.5474 | −3.5600 |
| $D\beta$ | 0.8369 | 0.8369 | −0.5474 | −1.1867 |

TABLE IV. Surface spins typical of region iv$_a$. $K/J=2.25$ and $L/J=2.25$, $\mathbf{k}=[0.0000, 0.2445]$, and the surface energy per unit cell is $-25.0471J$.

| $i\mu$ | $x_{i\mu}$ | $y_{i\mu}$ | $z_{i\mu}$ | $\phi_{i\mu}$ |
|---|---|---|---|---|
| $A\alpha$ | −0.7321 | −0.7321 | 0.6812 | 0.0000 |
| $A\beta$ | −0.7321 | −0.7321 | −0.6812 | −2.3734 |
| $B\alpha$ | −0.7321 | −0.7321 | 0.6812 | 0.0000 |
| $B\beta$ | −0.7321 | −0.7321 | −0.6812 | −2.3734 |
| $C\alpha$ | 0.8369 | 0.8369 | 0.5474 | −5.0965 |
| $C\beta$ | 0.8369 | 0.8369 | −0.5474 | −1.1867 |
| $D\alpha$ | 0.8369 | 0.8369 | 0.5474 | −5.0965 |
| $D\beta$ | 0.8369 | 0.8369 | −0.5474 | −1.1867 |

TABLE VI. Surface spins typical of region v. $K/J=3.00$ and $L/J=3.00$, $\mathbf{k}=[0.0000, -0.3078]$, and the surface energy per unit cell is $-29.3888J$.

| $i\mu$ | $x_{i\mu}$ | $y_{i\mu}$ | $z_{i\mu}$ | $\phi_{i\mu}$ |
|---|---|---|---|---|
| $A\alpha$ | 0.3654 | 0.3654 | 0.9308 | 0.0000 |
| $A\beta$ | 0.8442 | 0.8442 | 0.5360 | −4.1085 |
| $B\alpha$ | 0.8442 | 0.8442 | −0.5360 | 0.0000 |
| $B\beta$ | 0.3654 | 0.3654 | −0.9308 | −4.1085 |
| $C\alpha$ | 0.8800 | 0.8800 | 0.4750 | 2.0542 |
| $C\beta$ | 0.8800 | 0.8800 | −0.4750 | −2.0542 |
| $D\alpha$ | 0.8800 | 0.8800 | 0.4750 | 2.0542 |
| $D\beta$ | 0.8800 | 0.8800 | −0.4750 | −2.0542 |

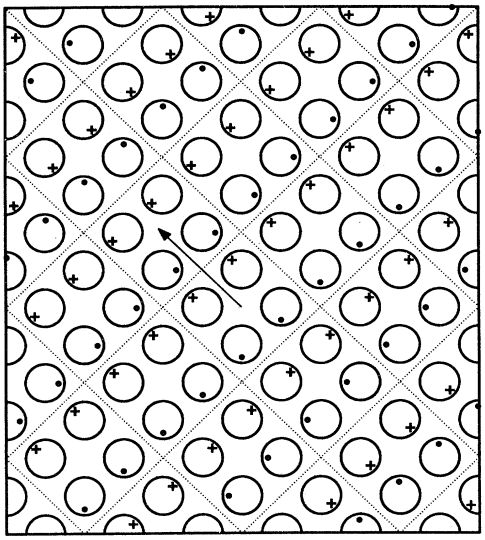

FIG. 6. A stereographic projection of the surface spins for a structure typical of regions iv corresponding to the spin parameters in Table IV. The dots denote spins pointing up, and the crosses spins pointing down. The arrow indicates the direction of **k** for this state. This surface state has a character similar to the bulk configuration, and is degenerate with the state pictured in Fig. 7.

rameter space near the i-iii-iv triple-phase points and more generally near all the commensurable-incommensurable phase boundaries. The exchange parameters describing the surface of EuTe may be near the i-iii-iv$_b$ triple-phase point (i.e., antiferromagnetic second-nearest-neighbor exchange and ferromagnetic nearest-neighbor exchanges[3]), and hence the small changes in the nearest-neighbor surface exchange expected to arise from temperature variations could generate large, experimentally observable shifts in **k**.

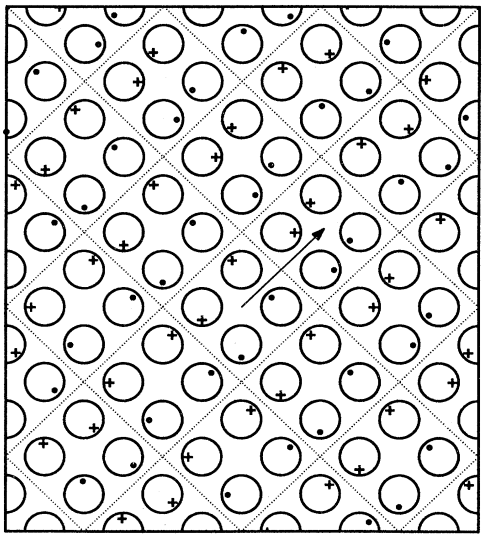

FIG. 7. A stereographic projection of the surface spins for a structure typical of regions iv corresponding to the spin parameters in Table V. The dots denote spins pointing up, and the crosses spins pointing down. The arrow indicates the direction of **k** for this state. This surface state has a character similar to the bulk configuration, and is degenerate with the state pictured in Fig. 6.

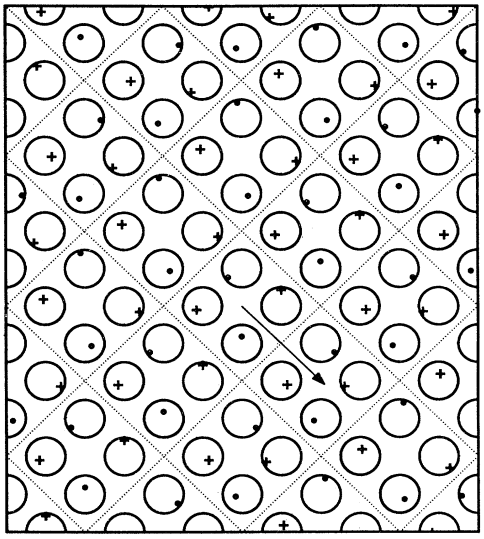

FIG. 8. A stereographic projection of the surface spins for a structure typical of regions v corresponding to the spin parameters in Table VI. The dots denote spins pointing up, and the crosses spins pointing down. The arrow indicates the direction of **k** for this state. A tendency towards a $z$-oriented nearest-neighbor square antiferromagnet ($z$-NNSA) is evident.

A notable feature of the results presented here is that the nearest-neighbor coupling $L$ between the surface and second layers is necessary for the stability of the incommensurable "frozen" spin waves. The surface-only nearest-neighbor exchange $K$, however, is not required for their stability. The region of stability of the incommensurable structures completely covers the regions IV of the commensurable phase-stability diagram, as one might expect, for these are exactly the regions of parameter space in which the spins are most "frustrated."

The magnetic structure of the surface should lead to Bragg diffraction peaks of low-energy electron diffraction experiments.[12,13] The intensity of the LEED beams at wave vector **Q** due to magnetic structure is proportional to the squared magnitude of the Fourier transform of the magnetization (spin structure), $|\mathbf{S}(\mathbf{Q})|^2$. Since some of the magnetic structure peaks do not correspond to chemical diffraction beams, they should be readily observed,[32] even with unpolarized electrons.

The positions of the beams diffracted by magnetic structures are designated by the vector **Q**. The magnitudes are measured in units of $[2\pi/b]$. The diffracted beams at $\mathbf{Q}=[2n, 2m+1]$ ($n$ and $m$ are integers) are those associated with the bulk-antiferromagnetic structure. The beams $\mathbf{Q}=[2n+1, 2m+1]$ are associated with NNSA and $z$-NNSA surface structure. The beams at $\mathbf{Q}=[2n,2m]$ are those associated with the chemical periodicity of the surface, and the ferromagnetic surface

structures as well. The beams due to incommensurable magnetic structure are those described by nonintegral $n$ or $m$. The structure factors calculated here are those of the surface layer only, and are calculated assuming only a single "frozen" spin wave.

Figure 9 is a plot of the structure factors for nonzero diffraction beams as a function of $L/J$ for $K/J=0$. The spin structures used in constructing this plot all have $\mathbf{k}$ along the $\Gamma$-to-$Y$ line, but the plot would be identical for $\mathbf{k}$ along the $\Gamma$-to-$Y'$ line. The solid line is the structure factor for the bulklike antiferromagnetic structure beams and the dashed-dotted line is the structure factor for the ferromagnetic structure beams. The dotted-line type corresponds to the beams diffracted by the incommensurable magnetic structure, which, for the choice of $\mathbf{k}$'s used here, are located at $\mathbf{Q}=[2n,2m]\pm\mathbf{k}$ for $2.8<L/J<4.0$ and at $\mathbf{Q}=[2n+1, 2m]\pm\mathbf{k}$ for $1.414<L/J<2.8$. Figure 10 is a plot of the endpoints of the $\mathbf{k}$ vectors of the incommensurable diffraction beams in Fig. 9. From $L/J=0$ to $L/J=1.414$ the surface structure is the bulk antiferromagnet. At $L/J=1.414$ the surface undergoes a first-order transition to an incommensurable state clearly shown by the jump in $\mathbf{k}$ seen in Fig. 10. As $L/J$ increases further, more and more of the scattering strength is at the incommensurable peaks. Simultaneously, however, $\mathbf{k}$ approaches the $\Gamma$ point. At $L/J=4.0$, the two incommensurable spots merge exactly at the zone center. Although in Fig. 9 this merging appears to be a first-order transition, it is not. It is the usual factor of 2 encountered in incommensurable-commensurable transitions. The distinct jump at $L/J=4.0$ appears because for $L/J<4.0$ the electrons are scattered into *two* spots with equal intensity, whereas for $L/J\geq 4.0$ the two peaks merge into *one*. The graph in Fig. 9 shows the structure factor for only one of the two equivalent spots.

Figure 11 is a plot of the magnetic structure factors for

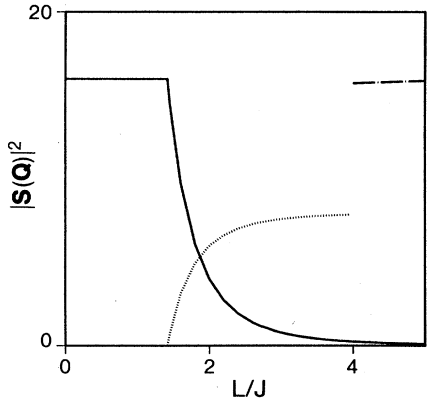


FIG. 9. The structure factor for the various diffraction beams as a function of $L/J$ for $K/J=0$. The solid line is the structure factor for one of the bulklike antiferromagnetic spots, the dashed-dotted line is for the surface ferromagnetic structure, and the dotted line is the structure factor for one incommensurable spot. At $L/J=4.00$, two incommensurable spots merge at the zone center, with a concomitant incommensurable-to-commensurable transition.

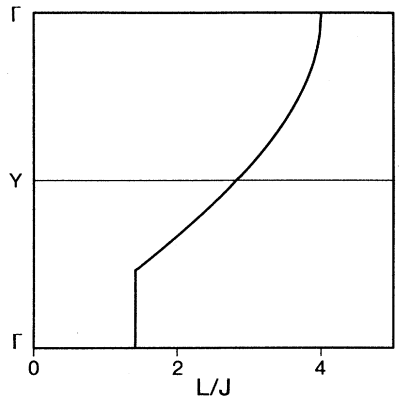


FIG. 10. The $\mathbf{k}$ vectors of the stable structures used to construct the plot in Fig. 9. The vectors originate at $\Gamma$ and end at the indicated point along the $\Gamma$-to-$Y$ line.

$L/J=3.00$ as a function of $K/J$ for the region near the $iv_a$-$v_a$ boundary. Here the $\mathbf{k}$ vectors of the incommensurable state were chosen to lie along the $\Gamma$-to-$Y'$ line. As in Fig. 9, the solid line is the magnetic structure factor for the bulklike diffracted beams; the dashed line is for the NNSA diffracted beams. The dashed-dotted–line type is the magnetic structure factor of the incommensurable diffraction beams at the points $\mathbf{Q}=[2n+1, 2m+1]\pm\mathbf{k}$. The dotted line is the structure factor for incommensurable beams at $\mathbf{Q}=[2n, 2m+1]\pm\mathbf{k}$. The structural transition at $K/J=2.56$ is clearly evident and appears to be smooth (second order).

Figures 9 and 10 indicated that the LEED patterns ex-

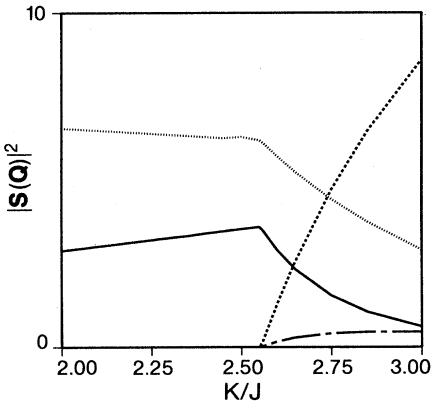


FIG. 11. The magnetic structure factor for $L/J=3.00$ as a function of $K/J$ for the minimum-energy state chosen to have $\mathbf{k}$ along the $\Gamma$-to-$Y'$ direction. The solid line is the structure factor for the bulklike diffraction beams at $\mathbf{Q}=[2n, 2m+1]$, the dashed line is the structure factor for the nearest-neighbor square-antiferromagnet-like (NNSA-like) beams at $\mathbf{Q}=[2n+1, 2m+1]$, the dotted line is the structure factor for incommensurable spots at $\mathbf{Q}=[2n, 2m+1]\pm\mathbf{k}$, and the dotted-dashed line is the structure factor for incommensurable spots at $\mathbf{Q}=[2n+1, 2m+1]\pm\mathbf{k}$. The structural transition upon crossing the $iv_a$-$v_a$ boundary at $K/J=2.56$ is clearly evident.

pected from the different structures can be very sensitive to relatively small changes in surface exchange integrals. LEED experiments performed on these materials, therefore, should be able to detect structural changes experimentally induced through temperature or pressure variations, which should affect the surface exchange integrals.

## IV. CONCLUSION

The phase-stability diagram of the simple classical Heisenberg Hamiltonian (1), found with trial states of the form (2), is remarkably complex. It shows entire regions of parameter space in which incommensurable spin structures are the stable ground state. Since *all* commensurable structures are included in this model, the incommensurable regions of the phase-stability diagram (Fig. 5) are certain to have incommensurable ground states, which may be the "frozen" spin waves of Eq. (2), or more complex *incommensurable* structures. These incommensurable surface structures are not stabilized by Fermi-surface–type effects, incommensurable or mean-field potentials, but rather are the result of competing nearest- and second-nearest-neighbor interactions. Nearest-neighbor coupling between the first and second layers seems to be necessary for the stability of the incommensurable structures.

The stable incommensurable "frozen" spin waves used in the calculation are of two basic types: one reminiscent of the bulk structure, type iv, and one which is suggestive of a mixture of the bulk and $z$-NNSA structures, type v. The fourfold degeneracy of the iv-type phase and the twofold degeneracy of the v-type phase are understood in terms of the coupling of the bulk: the $xy$ components of the iv-type phase surface spins do not feel the asymmetry of the bulk because the $z$ components of the spins in each layer are uniform. Differing from the properties of the iv-type phases, the v-type phases have nonuniform $z$ components of the surface spins and the transverse $xy$ components of the spins feel the asymmetry of the bulk (through their nonuniform magnitude), thereby lifting the degeneracy.

It is possible to choose the parameters $K/J$ and $L/J$ to stabilize the state of any $\mathbf{k}$ vector along the $\Gamma$-to-$Y$, or the $\Gamma$-to-$Y'$, line. In some regions of parameter space, which may also coincide with the parameters corresponding to EuTe, the $\mathbf{k}$ vector of the incommensurable stable state is very sensitive to small changes in $K/J$ and $L/J$.

Finally, since the LEED patterns of these antiferromagnets are expected to display additional diffraction beams caused by magnetic structure at the surface, the magnetic structure factors for several interesting cases were calculated. They revealed that the LEED pattern should be very sensitive to changes in surface exchange integrals. This sensitivity, expected in both location and intensity of the diffraction beams, should be easily observed.

## ACKNOWLEDGMENT

This research was supported, at the Lawrence Berkeley Laboratory, by the Director, Office of Energy Research, Office of Basic Energy Sciences, Materials Science Division, U.S. Department of Energy, under Contract No. DE-AC03-76SF00098.

[1]See, for instance, the various articles, in *New Developments in Semiconductors,* edited by P. R. Wallace, R. Harris, and M. J. Zuckermann (Noordhoff, Leyden, 1973).
[2]R. Ritter, L. Jansen, and E. Lombardi, Phys. Rev. B **8**, 2139 (1973).
[3]T. Janssen, Phys. Kondens. Mater. **15**, 142 (1972).
[4]P. W. Anderson, Phys. Rev. **115**, 2 (1959).
[5]M. A. Ruderman and C. Kittel, Phys. Rev. **96**, 99 (1954).
[6]B. Koiller and L. M. Falicov, J. Phys. C **8**, 695 (1975).
[7]C. Kittel, *Introduction to Solid State Physics,* 6th ed. (Wiley, New York, 1976), p. 444.
[8]*Magnetic Properties of Low-Dimensional Systems,* edited by L. M. Falicov and J. L. Morán-López (Springer-Verlag, Heidelberg, 1986).
[9]D. Castiel, Surf. Sci. **60**, 24 (1976).
[10]V. A. Grazhulis, A. M. Ionov, and V. F. Kuleshov, Phys. Chem. Mech. Surf. **4**, 503 (1986).
[11]R. E. De Wames, Phys. Status Solidi **39**, 437 (1970).
[12]L. M. Falicov and R. E. De Wames, Phys. Status Solidi **39**, 445 (1970).
[13]H. C. Siegmann, Phys. Rev. **17**, 37 (1975).
[14]R. H. Victora and L. M. Falicov, Phys. Rev. B **31**, 7335 (1985).
[15]L. E. Klebanoff, R. H. Victora, L. M. Falicov, and D. A. Shirley, Phys. Rev. B **32**, 1997 (1985).
[16]K. Sattler and H. C. Siegmann, Phys. Rev. Lett. **29**, 1565 (1972).
[17]M. Campagna, D. T. Pierce, K. Sattler, and H. C. Siegmann, Helv. Phys. Acta **47**, 27 (1974).
[18]S. F. Alvarado, E. Kisker, and M. Campagna, in *Magnetic Properties of Low-Dimensional Systems,* edited by L. M. Falicov and J. L. Morán-López (Springer-Verlag, Heidelberg, 1986), p. 52.
[19]V. A. Grazhulis (private communication).
[20]A. Werner, A. Arrott, and H. Kendrick, Phys. Rev. **155**, 528 (1967).
[21]W. M. Lomer, Proc. R. Soc. London, Ser. A **80**, 489 (1962).
[22]L. M. Falicov and D. R. Penn, Phys. Rev. **158**, 476 (1967).
[23]R. J. Elliott, Phys. Rev. **124**, 346 (1961).
[24]D. C. Chrzan and L. M. Falicov, Phys. Rev. Lett. **61**, 1509 (1988).
[25]D. de Fontaine, A. Finel, S. Takeda, and J. Kulik, in *Noble Metal Alloys,* edited by T. B. Massalski, W. B. Pearson, L. H. Bennett, and Y. A. Chang (The Metallurgical Society of AIME, Warrendale, PA, 1986), p. 49.
[26]M. E. Fisher and W. Selke, Philos. Trans. R. Soc. London **302**, 1 (1981).
[27]S. Aubry and P. Y. Le Daeron, Physica (Utecht) D **8**, 381 (1983).
[28]T. Janssen and A. Janner, Adv. Phys. **36**, 519 (1987).

[29]There are eight possible antiferromagnetic {111} structures. The configuration chosen here utilizes the (111) planes and has the bulk spins pointing in the $z$ direction. While specific details of the calculation differ for other choices, the physical conclusions are identical for all eight structures.

[30]V. G. Tissen and E. G. Ponyatovskii, Pis'ma Zh. Eksp. Teor. Fiz. **46**, 287 (1987) [JETP Lett. **46**, 361 (1987)].

[31]D. C. Mattis, *The Theory of Magnetism* (Harper and Row, New York, 1965).

[32]P. Palmberg, R. E. De Wames, and L. Vredevoe, Phys. Rev. Lett. **21**, 682 (1968).